

**Characterisation of timber joists-masonry connections in double-leaf cavity walls – Part 2  
Mechanical model**

Arslan, O.; Messali, F.; Smyrou, E.; Bal, E.; Rots, J. G.

**DOI**

[10.1016/j.istruc.2024.107165](https://doi.org/10.1016/j.istruc.2024.107165)

**Publication date**

2024

**Document Version**

Final published version

**Published in**

Structures

**Citation (APA)**

Arslan, O., Messali, F., Smyrou, E., Bal, E., & Rots, J. G. (2024). Characterisation of timber joists-masonry connections in double-leaf cavity walls – Part 2: Mechanical model. *Structures*, 68, Article 107165. <https://doi.org/10.1016/j.istruc.2024.107165>

**Important note**

To cite this publication, please use the final published version (if applicable).  
Please check the document version above.

**Copyright**

Other than for strictly personal use, it is not permitted to download, forward or distribute the text or part of it, without the consent of the author(s) and/or copyright holder(s), unless the work is under an open content license such as Creative Commons.

**Takedown policy**

Please contact us and provide details if you believe this document breaches copyrights.  
We will remove access to the work immediately and investigate your claim.



## Characterisation of timber joists-masonry connections in double-leaf cavity walls – Part 2: Mechanical model

O. Arslan<sup>a,b,\*</sup>, F. Messali<sup>a</sup>, E. Smyrou<sup>b</sup>, I.E. Bal<sup>b</sup>, J.G. Rots<sup>a</sup>

<sup>a</sup> Faculty of Civil Engineering and Geosciences, Delft University of Technology, Delft, the Netherlands

<sup>b</sup> Research Centre for Built Environment NoorderRuimte, Hanze University of Applied Sciences, Groningen, the Netherlands

### ARTICLE INFO

#### Keywords:

Unreinforced masonry  
Timber-joist connections  
Cavity walls  
As-built connections  
Strengthened connections  
Mechanical modelling

### ABSTRACT

The seismic assessment of the out-of-plane (OOP) behaviour of unreinforced masonry (URM) buildings is essential since the OOP is one of the primary collapse mechanisms in URM buildings. It is influenced by several parameters, including the poor connections between structural elements, a weakness highlighted by post-earthquake observations. The paper presents a mechanical model designed to predict the contributions of various resisting mechanisms to the strength capacity of timber-joist connections in masonry cavity walls. The research presented in this paper considers two different failure modes: joist-wall interface failure, and OOP rocking behaviour of the URM walls. Consequently, two mechanical models are introduced to examine these failure modes in timber-joist connections within masonry cavity walls. One model focuses on the joist-wall interface failure, adopting a Coulomb friction model for joist-sliding further extended to incorporate the arching effect. The other model investigates the OOP rocking failure mode of walls. The combined mechanical model has been validated against the outcomes of an earlier experimental campaign conducted by the authors. The considered model can accurately predict the peak capacity of the joist connection and successfully defines the contribution of each mechanism in terms of resistance at failure.

### 1. Introduction

The seismic behaviour of unreinforced masonry (URM) structures is primarily governed by their ability to redistribute horizontal loads among structural elements, particularly from walls subjected to out-of-plane (OOP) loading to those subjected to in-plane (IP) loading, which is commonly referred to as box-behaviour [1]. Specifically, the effectiveness of the connections between walls and diaphragms is crucial in preventing OOP failures and exploiting the structure's maximum resistance.

URM buildings with lack of adequate connections show high vulnerability to OOP collapse, as revealed by post-earthquake structural observations in various world regions, such as those conducted after the 1997 Umbria-Marche earthquake in Italy [2], the 2009 L'Aquila earthquake in Italy [3], the 2011 Canterbury earthquake in New Zealand [4], or the 2015 Gorkha earthquakes in Nepal [5]. This is also expected to be a critical issue in Groningen, a province in the north of the Netherlands where human-induced earthquakes caused by gas extraction have occurred in the last decades [6]. The building stock in the region is

commonly constituted by either single-wythe or double-wythe calcium-silicate and clay brick URM walls, timber floors and lack of any specific seismic detailing such as connections between structural elements [7–9]. Additionally, cavity walls whose leaves are often connected by insufficient or corroded steel ties are often used. However, until now, little research has been carried out to characterise the seismic behaviour of connections between structural elements in typical Groningen houses, especially wall-to-diaphragm connections.

Keeping this aim in mind, an experimental campaign was conducted at Hanze University of Applied Sciences to provide benchmarks for the definition and validation of mechanical models for timber-diaphragm connections. The campaign, presented in [10], aimed to provide a complete structural characterisation of timber joists to URM cavity walls in both as-built and strengthened conditions under cyclic axial loading. Two different failure modes were observed: (i) failure at the joist-wall interface, with a joist-sliding failure mode that included partial joist-to-wall interaction in case of weak as-built joist-masonry connections, and (ii) OOP rocking failure of the wall for retrofitted over-resistant connections. The former mechanism depended on the

\* Corresponding author at: Faculty of Civil Engineering and Geosciences, Delft University of Technology, Delft, the Netherlands

E-mail addresses: [o.arslan@tudelft.nl](mailto:o.arslan@tudelft.nl), [o.arslan@pl.hanze.nl](mailto:o.arslan@pl.hanze.nl) (O. Arslan), [F.Messali@tudelft.nl](mailto:F.Messali@tudelft.nl) (F. Messali), [e.smyrou@pl.hanze.nl](mailto:e.smyrou@pl.hanze.nl) (E. Smyrou), [i.e.bal@pl.hanze.nl](mailto:i.e.bal@pl.hanze.nl) (I.E. Bal), [J.G.Rots@tudelft.nl](mailto:J.G.Rots@tudelft.nl) (J.G. Rots).

<https://doi.org/10.1016/j.istruc.2024.107165>

Received 29 January 2024; Received in revised form 13 August 2024; Accepted 23 August 2024

Available online 28 August 2024

2352-0124/© 2024 The Authors. Published by Elsevier Ltd on behalf of Institution of Structural Engineers. This is an open access article under the CC BY license (<http://creativecommons.org/licenses/by/4.0/>).

cohesion and friction between the timber joist and the masonry, as well as on the arch effect activated due to the joist-to-wall interaction. The latter failure mechanism was characterised by the rocking behaviour of either one or both leaves of the wall.

A summary of studies that proposed mechanical models for the frictional behaviour of joist-wall connections and for the rocking behaviour of URM walls is provided. The main objective of this review is to identify mechanical models that account for not only pure sliding of the connection or rocking of the URM walls but simultaneously incorporate an arching effect.

### 1.1. Literature review of frictional behaviour of joist-to-wall connections

The failure of timber-joist connections is often governed by their shear behaviour: when the shear force applied at the interface of the part of the joist embedded in a URM wall exceeds the frictional capacity of the connection, sliding of the joist occurs. Coulomb classified two types of friction as follows: (i) static friction, which is the resistance until starting the relative motion, and (ii) dynamic friction, which concerns the resistance when the surfaces move with respect to one another.

The static friction coefficient can be computed as the maximum tangential force that develops before the onset of the sliding mechanism divided by the normal load acting on the interface. In contrast, the resisting force due to dynamic friction can be described in terms of the residual resisting force, which is achieved after the force drop due to the activation of sliding. In the study of Suh & Turner [11], static and dynamic friction were compared for the dry materials. It was concluded that the dynamic friction coefficient was smaller than the static friction coefficient, generally of the order of 25 %. Another study by Doherty [12], evaluated the performance of URM connections containing damp proof course membranes under dynamic loading in order to assess their seismic integrity. In addition, he compared the dynamic friction coefficient determined from the experiments conducted by the author with the quasi-static friction coefficient derived and proposed by Griffith & Page [13]. It was highlighted that the quasi-static friction coefficient was not more than 20 % higher than the dynamic friction coefficient.

Casapulla et al. [14] conducted a study on the simple overturning mechanism of a masonry wall weakly connected to the timber diaphragm. They defined a priori a failure mode based on the frictional resistance at the support of the timber diaphragm. This was represented as a cohesionless Coulomb's law so that the capacity of the connection is limited by a horizontal friction force.

The physical characteristics of the contact surfaces can affect cohesion and friction coefficient. Casapulla et al. [14] investigated the stabilising role of the frictional resistance in presence of a simply inserted horizontal diaphragm. A value of friction coefficient equal to 0.1 was assumed for light horizontal diaphragms, 0.3 for intermediate diaphragms, and 0.6 for heavy diaphragms. The sensitivity of the load multiplier (i.e. the factor by which the earthquake ground motion should be scaled to determine failure of the structure) with respect to the friction coefficients was studied. It was found that when a joist is inserted in a masonry pocket of a URM wall, an increase in the seismic masses associated with heavier floors reduces the load multiplier of the walls.

The joist-sliding failure mode was recently studied by Almeida et al. [15], who conducted an experimental campaign with cyclic triplet tests between mortar and timber units. Friction was described as a surface force that restrained the sliding motion of bodies. Three assumptions were made: friction is (i) independent of the normal area of contact, (ii) proportional to the normal force, and (iii) independent of the sliding speed. The first assumption had as consequence that the contribution of cohesion was neglected.

The static friction force corresponded to a maximum shear force, which developed before the onset of sliding of the joist. In contrast, the resisting force due to dynamic friction was described in terms of residual resisting force, which was achieved after the force dropped due to the

activation of sliding. The study concluded that the dynamic and static friction coefficients were similar for mortar-timber specimens.

Besides dry friction, cohesion contributes to the bond at the interface between timber and masonry, playing an important role in the definition of the peak force and of the post-cracking hysteric behaviour [16]. Although the cohesion bond between brick and mortar was commonly studied in the literature [17–19], only few studies have focused on the cohesion between timber and masonry [20,21]. A Coulomb type of representation can be adopted to determine the friction and cohesion bond between masonry and timber (Fig. 1a). The Coulomb friction criterion [22] is based on a linear failure envelope to determine the critical combination of shear and normal stress that will cause failure. The ultimate shear strength at the interface between timber and masonry at a particular level of normal stress can be calculated by the Coulomb criterion (1), as seen in Fig. 1b. The post-peak phase is characterised by cohesion softening, followed by a plateau representing residual dry friction.

$$\tau = c + \mu \cdot \sigma_N \quad (1)$$

### 1.2. Literature review of arching effect

As mentioned above, the joist-wall interface failure observed in the experimental campaign conducted by the authors [10] was characterized by sliding of the joist. The resistance of the connection was affected by the interaction of the joist to the wall, as an arching mechanism was activated while deforming OOP. The arch effect increases the level of lateral confinement at the timber-wall interface and hence affects frictional behaviour. No studies in the literature focused on frictional behaviour with arching effect for timber-masonry connections to the knowledge of the authors. However, the arching effect on masonry structures and how it may affect the force capacity of the walls have been studied extensively in the literature [23–26].

The strength capacity of masonry walls can be affected by the arching effect when URM walls are bounded by relatively rigid elements [25]. Hence, where vertical displacement is restrained, fixed-fixed boundary conditions may induce arching effects under OOP loading. Nils Royen's work, dating back to 1937, can be considered the foundation for the arch effect in the compressive response of unreinforced masonry (URM) walls under vertical loading, as noted by Magenes [27]. Subsequently, similar approaches have been followed by other authors in the following decades [28–31].

Paulay and Priestley [32] introduced a simplified procedure that relies on the elastic buckling behaviour for the OOP response of masonry walls, particularly for one-way vertical spanning URM walls. This procedure is based on the exact solution for the compressive response of masonry walls originally developed by Sahlin [30]. The simplified analytical model is developed to define the load-deflection ( $P-\Delta$ ) relationship for masonry walls. Fig. 2 illustrates the behaviour of a slender unreinforced wall subjected to an applied vertical load.

The vertical load,  $P$ , and corresponding displacement,  $\Delta$ , can be computed according to Paulay and Priestley [32], as follows:

$$\Delta = 0.5 \times t_w \times \left( y - \sqrt{y^2 - \frac{f_c}{6E} \left( \frac{h}{t_w} \right)^2} \right) \quad (2)$$

$$P = 0.75 \times f_c \times t_w \times \left( y + \sqrt{y^2 - \frac{f_c}{6E} \left( \frac{h}{t_w} \right)^2} \right) \quad (3)$$

$$y = \frac{1}{2} - \frac{e}{t_w} \quad (4)$$

where  $t_w$  is the thickness of the wall,  $y$  is the dimensionless distance from the extreme compression fibre at the top and bottom sections of the wall to the line of action of the load,  $P$ ,  $h$  is the height of the wall and  $e$  is

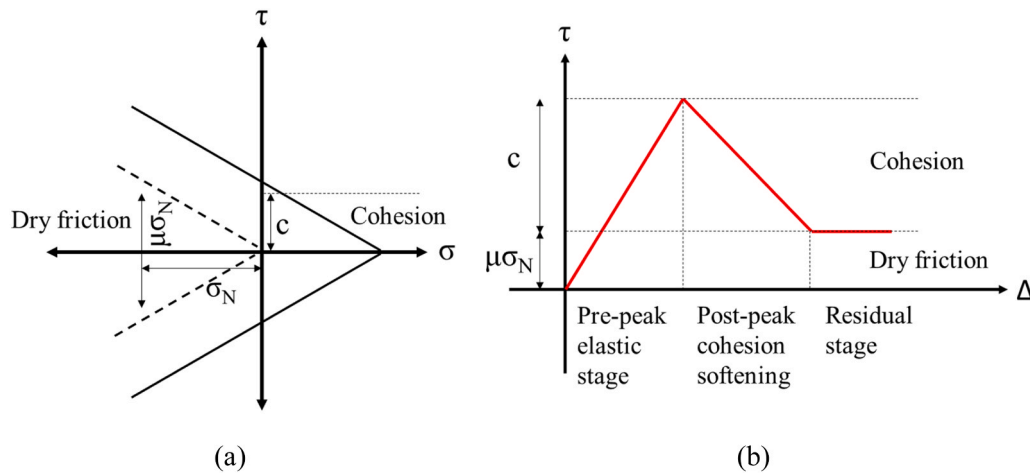


Fig. 1. Definition of cohesive-frictional behaviour in shear: Coulomb friction law (a), and Coulomb friction and cohesion softening for interfaces subjected to shear and compression (b).

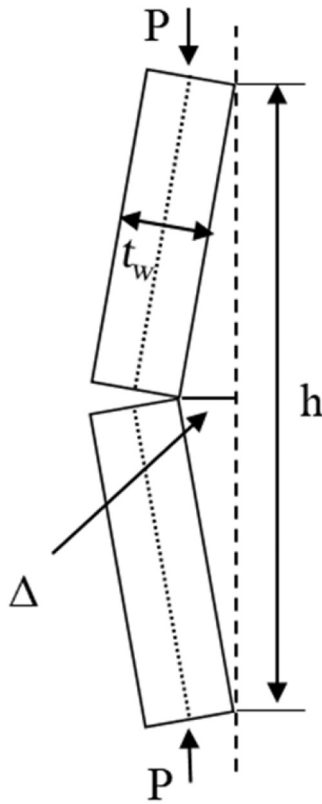


Fig. 2. Schematic presentation of the behaviour of a slender URM wall subjected to vertical load from Paulay and Priestley [32].

the eccentricity of the axial load. An increase in the lateral displacement,  $\Delta$ , leads to an increase of the bending moment at midspan. It should be noted that the lateral displacement,  $\Delta$ , or the load,  $P$ , can be obtained by differentiating Eqs. (2) or (3), respectively, for a given stress value at the extreme compression fibre at mid-height,  $f_c$ .

### 1.3. Literature review of rocking behaviour of URM walls

The rocking behaviour of rigid blocks or assemblies has been widely studied in the literature [23,33–36] since it is one of the most common out-of-plane (OOP) failure mechanisms for URM walls. The type and quality of masonry, geometry of the wall, boundary conditions and

magnitude of the vertical load can influence the rocking failure mechanism [37]. The simplest configuration is represented by URM cantilever walls. When subjected to OOP loading, such walls first crack along the base of the wall and then undergo rocking behaviour. For URM cantilevers, the static overturning force can be simply computed assuming zero tensile strength. When the URM walls are supported also at the top (one-way vertical spanning walls), cracks develop at top, bottom and approximately mid-height of the wall. The resulting force due to vertical bending moment at a specific height of wall can be calculated as recommended in the Australian Masonry Standards, AS3700 [38].

The assessment of the OOP failure of URM walls has been studied mostly for single leaf walls [12,33,39–42]. Doherty et al. [12] proposed a bilinear curve to represent the OOP force-displacement behaviour of walls, by assuming infinite material stiffness for the rigid bodies in which the wall is divided after cracking. Griffith et al. [41] conducted an experimental program to produce experimental evidence and support the model proposed by Doherty et al. [12]. During the experimental campaign, a total of 14 one-way vertically spanning URM walls were tested. The load was applied at mid-height of the walls by means of an actuator. The boundary conditions represent a simply supported wall with a vertical load at the top-edge of the wall face. Force-displacement relationships were computed via both the linear elastic theory and the rigid body theory. However, both equations consider only a single wall since cavity walls have a complex dynamic behaviour due to the presence of the load-bearing leaf and the non-load-bearing leaf connected by cavity wall ties.

Tomassetti et al. [34] proposed a static force-displacement relationship for the OOP analysis of one-way vertical spanning strip cavity walls. The model assumes that the cavity wall ties provide effective connection between the two leaves. In the study of Tomassetti et al. [34], the seismic behaviour of vertically spanning URM cavity walls subjected to out-of-plane movements is defined by a bilinear force-displacement model, derived from a nonlinear rigid-body kinematic analysis. The model represents an upper bound of the OOP static force capacity, which is the total rigid body force,  $F_{RP} = F_c + F_{0,iw} + F_{0,ow}$ , associated with the sum of the two rigid body mechanism forces of the two walls, and the coupling force of the embedded ties. The deformation capacity is represented by the instability displacement,  $u_{ins}$ , which is the maximum wall displacement.

The linear elastic response of the OOP one-way bending is calculated by adopting the equilibrium method according to plastic analysis principles. First, the cracking force is defined based on the identified boundary conditions. Hence, only one level of stiffness is associated with calculating the cracking force due to the formation of one hinge for the

pinned-pinned condition. After the formation of the horizontal crack at the mid-height of the wall, the rocking behaviour fully develops. The formation of three hinges, which are at the wall bottom (A-A'), mid-height (B-B') and top (C-C') can be seen in Fig. 3. The rigid bodies rotate around the pivot points A', B and C'.  $\alpha_1$  and  $\alpha_2$  represent the geometric angles for defining the slenderness of the two rigid bodies above and below the mid-height crack of the wall.  $W_1$  and  $W_2$  are the weights of the two rigid bodies below and above, respectively.  $\sigma_{v0}$  is the vertical overburden stress applied with eccentricity,  $e$ .  $h_1$  and  $h_2$  are the heights of the two rigid bodies below and above, respectively.

Due to the hinges, the wall can undergo large displacement. The proposed model also considers the eccentricity due to migration of the top resultant overburden force along the top edge of wall. Regarding the bilinear curve, as seen in Fig. 4, rigid force,  $F_o$ , and the instability displacement,  $u_{ins}$ , are calculated by using the following equations, respectively:

$$F_o = \frac{2}{h_1} (W + \sigma_{v0} \cdot t_w) \cdot t_w + \frac{\sigma_{v0} \cdot t_w}{h - h_1} (t_w + 2e) \quad (5)$$

$$u_{ins} = \frac{\frac{2}{h_1(W + \sigma_{v0} \cdot t_w)} + \frac{\sigma_{v0} \cdot t_w (t_w + 2e)}{h - h_1}}{\frac{2}{h_1(W + \sigma_{v0} \cdot t_w)} + \frac{2\sigma_{v0} \cdot t_w}{h - h_1}} \quad (6)$$

where  $h_1$  is the panel height where the maximum tensile stress equals the masonry flexural strength,  $\sigma_{v0} \cdot t_w$  is the overburden force,  $W$  is the weight of masonry,  $t_w$  is the thickness of the masonry and  $e$  is eccentricity. The coupling force contribution of ties in cavity wall can be calculated as follows:

$$F_c = 2 \cdot V_t \cdot t_w \cdot \frac{h}{h_1 \cdot h_2} + 2 \cdot M_t \cdot \frac{h}{h_1 \cdot h_2} \quad (7)$$

$$V_t = \sum_1^n V_i \quad (8)$$

$$M_t = \sum_1^n M_i \quad (9)$$

where  $V_t$  and  $M_t$  are the sum of the "n" tie plastic moments and the corresponding shear forces at the inner leaf edge interface, respectively. As shown in Fig. 4, the force capacity of the cavity wall specimens can be defined as the sum of the cracking force of the two leaves (considered independent) and the coupling force:

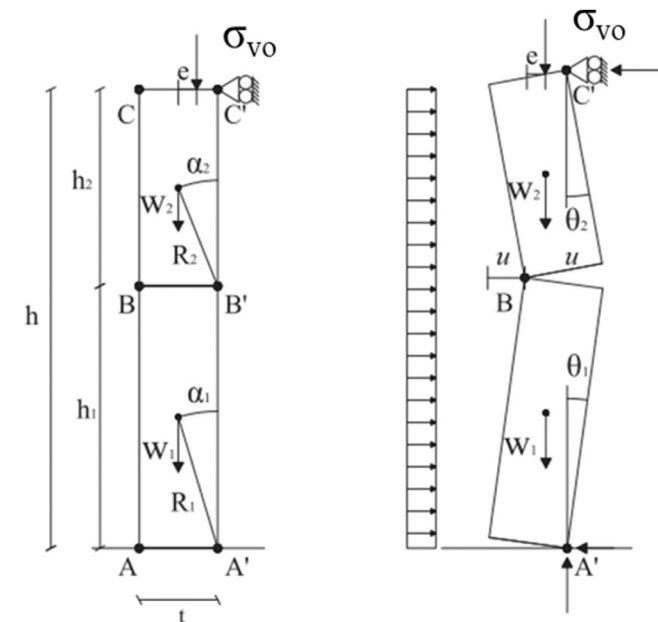


Fig. 3. Rocking behaviour for one-way vertical spanning strip walls: geometry at rest (left) and deformed shape (right) from Tomassetti et al. [34].

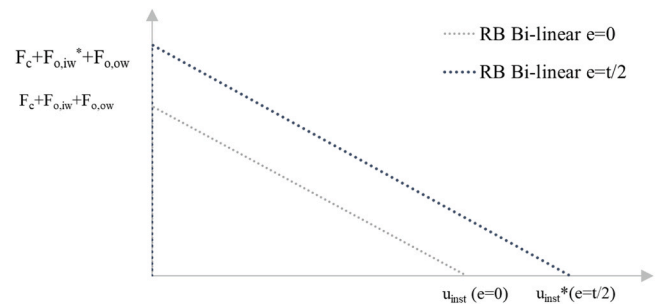


Fig. 4. Bilinear envelope curve for the force-displacement curve of a one-way spanning wall, proposed by Tomassetti et al. [34].

$$F_{RP} = F_{o,iw} + F_{o,ow} + F_c \quad (10)$$

### 1.4. Main objectives and approach

Considering the observed failure modes from the experimental campaign [10], a mechanical model that takes into account the frictional behaviour and arching effect is selected amongst the models described in the literature. The adopted model is based on the Coulomb criterion with the addition of arching effect from the joist-to-wall interaction. Regarding the rocking failure mode, the model proposed by Tomassetti et al. [34] is used to predict the rocking capacity of the cavity wall system. Section 2 summarises the experimental campaign conducted by the authors [10], including the specimen geometry, test setup, and the results. Section 3 presents the adopted mechanical modelling for (i) joist-wall interface failure mode and (ii) rocking failure modes. Section 4 compares the values of the force capacity of the connections predicted via the mechanical model with the experimental results, grouping the results by type of connection in both unstrengthened and strengthened conditions.

## 2. Experimental campaign

This section provides a summary of the experimental campaign conducted by the authors [10]. The campaign aimed to provide a better understanding and characterization of the cyclic axial behaviour of timber joist-masonry connections. This involved reproducing cavity walls with timber joists in both as-built and strengthened conditions, with different variations, including two tie distributions, two pre-compression levels, two different as-built connections, and one strengthening solution. The specimens were built at the BuildinG laboratory. Each specimen consisted of a cavity wall with metal ties and a timber joist laid in a pocket in the inner leaf of the wall (Fig. 5). The cavity wall was composed of an inner load-bearing leaf made of calcium silicate brick masonry (CS) and an outer non-load-bearing leaf made of clay brick masonry (CB) with an 80 mm cavity (Figure 4.4). Timber joists were made of C24 timber [44], similar to those used in the study carried out by Mirra et al. [45]. Timber joists in real buildings may have various types of imperfections that are not investigated here but could significantly affect the overall behaviour.

The wallet specimens were tested on an out-of-plane test setup. The test setup was composed of a stiff reaction frame, two air bellows and an actuator (Fig. 6). The specimens were loaded via the joist with the electric actuator, which was positioned over the joist. It should be noted that due to the way the free end of the joist was connected to the actuator, rotation of the joist was prevented. A vertical dead load of 100 kg was applied to the middle of the joist to simulate the self-weight of the portion of the floor supported by the joist.

The specimens were subjected to vertical pre-compression via two air bellows to simulate the effect of load-bearing walls acting on the inner leaf of the masonry structure. The top horizontal edge of the inner leaf

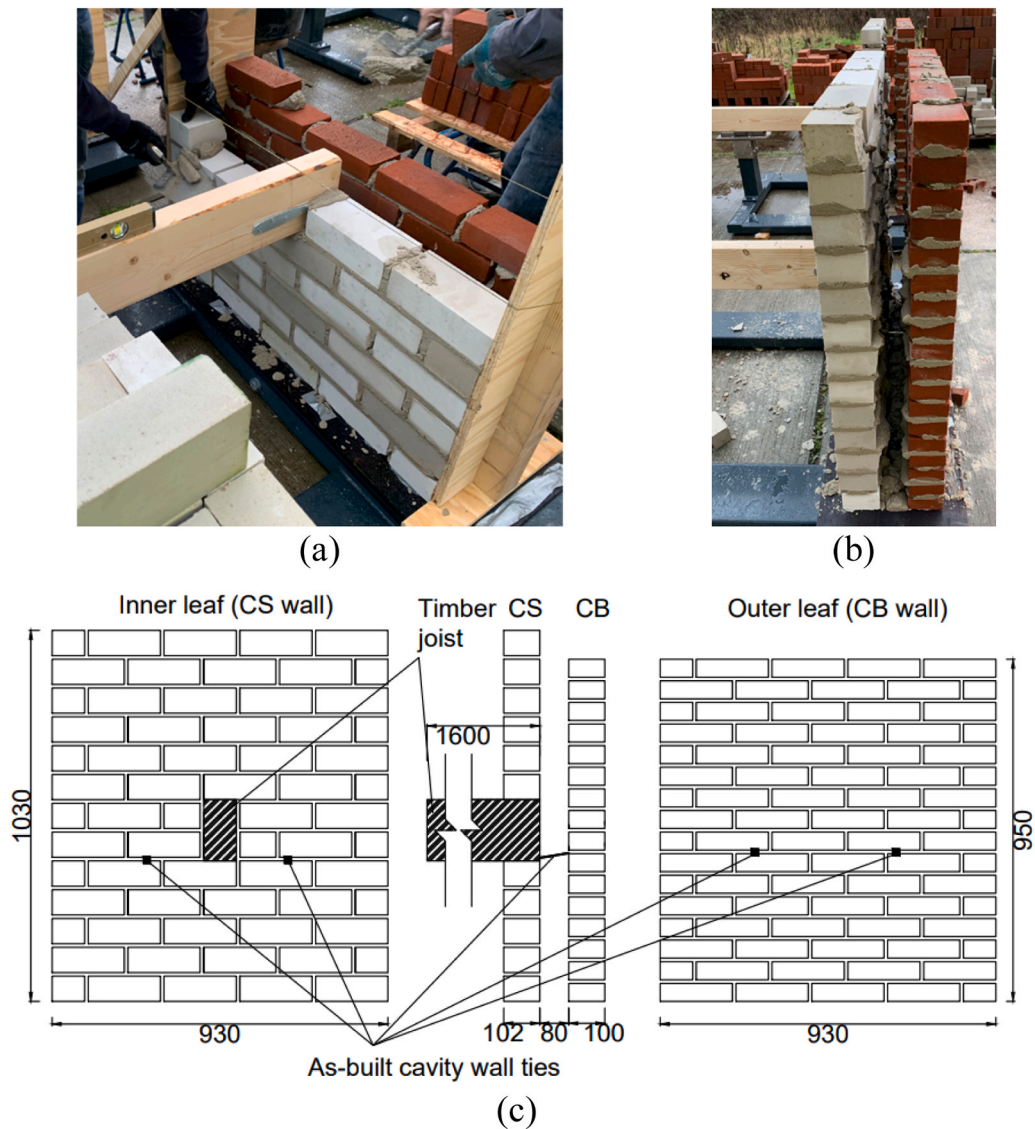


Fig. 5. The wallets during construction (a and b), and geometry of a specimen with two as-built cavity-wall ties (dimensions are in mm).

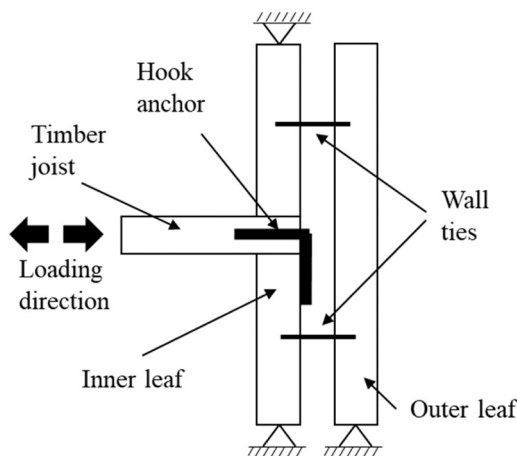


Fig. 6. Schematic view of the test setup.

was restrained against the vertical translation due to the presence of the air bellows to apply the overburden. Because of that, the out-of-plane boundary condition of the inner leaf was treated as a simply-

supported system in which the rotations at both the top and bottom of the wall were free. While the boundary condition of the outer veneer was treated as a cantilever system, in which the top edge of the wall was free to rotate and translate. The boundary condition of the specimens is schematically shown in Fig. 7. The vertically fixed restraint condition may induce arching effect in the case of OOP rocking of the inner leaf.

The as-built specimens were made up of two different connections: the masonry pocket connections labelled as J1, J3 and J5 (where the timber joist was simply placed in the inner leaf) and the hook anchor connections, labelled as J2, J4 and J6. After completing the testing of timber joist-cavity wall specimens in as-built condition, the six walls (J1, J2, J3, J4, J5 and J6) were retrofitted by connecting the outer leaf and the timber joist with helicoidal bars and retested, which were named by adding “T” to the names of the corresponding as-built specimens, i.e., TJ1 to TJ6. The specimens with masonry pocket connection exhibited a joist-sliding failure mode, which included partial joist-to-wall interaction, while the specimens with hook anchor and the strengthened specimens exhibited a rocking failure mode. The former failure mode was characterised by the joist sliding, causing diagonal cracks propagating from the joist. The latter failure mode showed an out-of-plane rocking mechanism. As an example of the rocking behaviour, experimental results of a strengthened specimen were selected to illustrate the

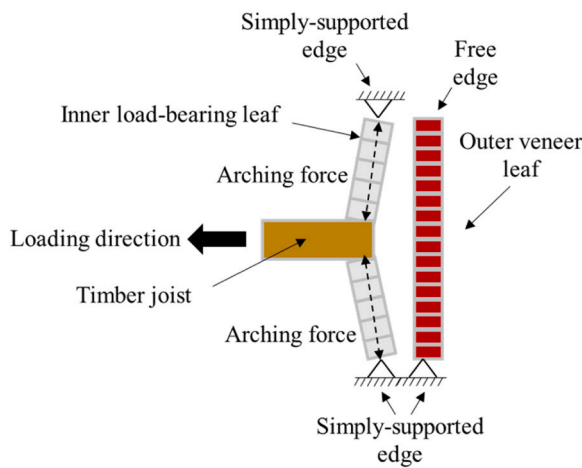


Fig. 7. Schematic description of the arching effect mechanism.

OOP displacement at the middle height and the top of the outer leaf, as well as the deformed shape at the end of the test. Additionally, a photograph capturing the corresponding moment during the test is included (Fig. 8).

It's necessary to consider scenarios where the arching effect becomes relevant in real buildings. Such situations can take place when load redistribution occurs above the connection as a result of the OOP rocking mechanism of the wall. This redistribution may develop in case of stiff portions of masonry above the connections so that local uplifting is prevented. This paper proposes a novel method to assess the timber-joist connections where the Coulomb friction model is adopted and further extended to include the arching effect using the model proposed by Paulay and Priestley [32].

### 3. Mechanical model

Two mechanical models are introduced to examine different failure modes in timber-joist connections within masonry cavity walls. The first mechanical model is based on the Coulomb criterion with the addition of the arching effect from the joist-to-wall interaction. The other model investigates the rocking failure mode, applying the model proposed by Tomassetti et al. [34] to predict the strength capacity of the connections

whose experimental performance was conducted by the authors [43]. The study aims to identify the contributions of various resisting mechanisms to the force capacity of the connection.

#### 3.1. Frictional behaviour of joist-to-wall connections

As highlighted in Section 1, there has been no prior research that specifically addresses the development of a model for a joist-sliding failure mode that included partial joist-to-wall interaction. The model presented in this study is designed to bridge this gap in knowledge. It should be kept in mind, however, that the interaction of the wall with the joist also depends on wall dimensions and boundary conditions; hence, the findings reported here are limited to the conditions previously tested by the authors.

In the experiments described in [10], it is observed that an additional vertical force, other than the pre-compression setup at the beginning of the test, is introduced at the joist-wall interface [10]. In the test setup, the displacements of the horizontal top and bottom edges of the specimens are restrained. As a consequence, the wall is vertically confined. Hence, when the middle of the wall is displaced in the out-of-plane (OOP) direction, the deformation of the specimen and the uplifting resulting from cracking causes an increase in the axial vertical force, affecting the capacity of the connection. The additional resistance created by this restraining effect is function of the horizontal bending caused by the displacement imposed at mid-height of the wall. This leads to a migration of the neutral axis in the cracked wall sections, and hence introduces an elongation along the centroidal axis and results in greater compressive forces vertically. The elongation can be related to the horizontal displacement of the wall at the pocket where the timber joist was inserted through simple geometric observations. This effect, caused by bulging of the mid-height of the wall following the joist, is the arching effect.

It should be noted that this phenomenon is noticeable only when the vertical movement of the specimen is either fully or partially restrained. This may happen in the case of walls at lower levels in buildings and confined at the top by rigid diaphragms, which usually are vertically strong and heavier, imposing larger compression and thus strength [46]; the force redistribution following the cracking of the walls may cause the bespoke arching action. Conversely, the arching effect may not be taken into account if a structure is characterised by load-bearing URM walls with flexible diaphragms and, hence, less rigid restraints also

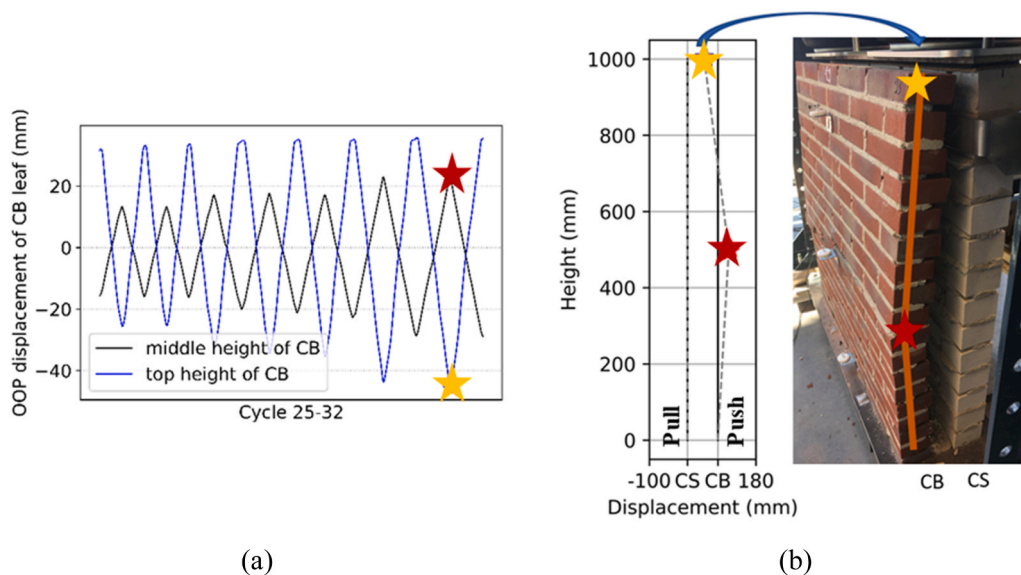


Fig. 8. OOP rocking behaviour of a strengthened specimen. OOP displacement at the middle height and at the top of the outer leaf (a), and the deformed shape at the end of the test with a photograph of the corresponding moment (b).

vertically [25,47,48]. Additionally, it should be noted that the presence of the mortar surrounding the joist within the pocket allowed the arching forces to be transferred at the interface, which would not occur in case of a physical gap between the top side of the joist and the intersection masonry wall.

The additional resistance determined by the arching effect is schematically illustrated in Fig. 9. The curve expresses the relation between the horizontal force transferred by the timber joist to the masonry and the relative displacement between the joist and the wall. Without the arching effects, the force-deformation curve of a timber joist – wall connection would be based on Coulomb’s law consisting of two contributions, one due to cohesion ( $F_{co}$ ) and one to friction and the initial level of pre-compression ( $F_{if}$ ),  $F_{NP} = F_{co} + F_{if}$ . In the case of vertically restrained conditions, an arching effect is triggered as mentioned earlier, adding to the strength, and resulting an additional capacity,  $F_{af}$ . This modified curve, highlighted in blue in Fig. 9a, exhibits increased stiffness and strength,  $F_{MP}$ , compared to the unrestrained conditions.

The additional arching force is proportional to the OOP displacement at the mid-height of the inner leaf. For this reason, it is related to the level of connectivity between the joist and masonry. When the joist and the wall are well connected, such as in the initial elastic branch, the OOP

displacement at the mid-height of the inner leaf is equal to the horizontal displacement of the timber joist. For this reason, the maximum contribution of the arching effect is obtained at the end of the elastic region where the peak force is attained. After the peak, the level of connectivity between the joist and the wall decreases, and relative displacements due to sliding between the two structural elements increases. The OOP displacements of the wall then become gradually smaller than those of the joist, reducing the effect of the arching force. The post-peak phase of the proposed curve is, therefore, characterised by a softening behaviour attributed to the cohesion softening behaviour and the fading out of the arching effect, followed by a plateau due to the dry friction only.

The conditions for the activation of the arching effect are illustrated in Fig. 10. In this schematic illustration, the height of the thrust line,  $h'$ , is the path followed by the resultant of the forces acting on an arch across its span. When a unique displacement,  $u$ , of joist and inner leaf is observed thanks to the initial strong bond between masonry and timber, the arching effect is activated, introducing an elongation along the centroidal axis and hence leading to additional compressive normal stresses at the joist-wall interface. This increases the frictional capacity of the joist-masonry connection. The sliding of the joist starts when this force is exceeded due to the absence of anchors between the joist and the

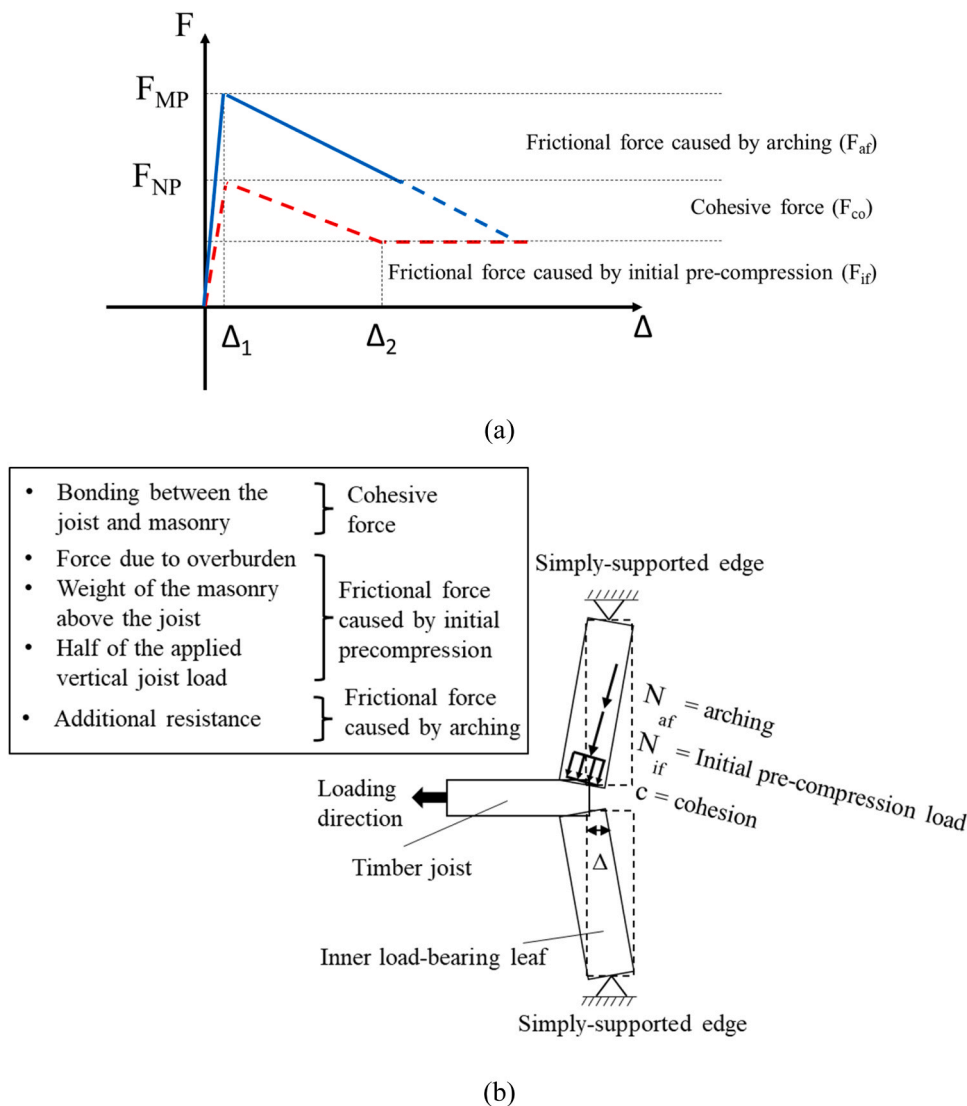


Fig. 9. Proposed envelope curve compared to the conventional Coulomb model. The vertical axis indicates OOP force transferred by the timber joist to the wall, while the horizontal axis indicates the relative displacement between the joist and wall (a). Schematic used to compute the normal force acting at the interface between masonry and joist (b).

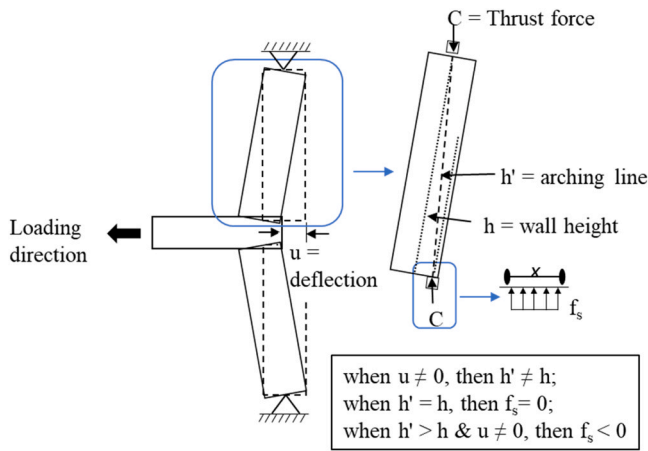


Fig. 10. Schematic representation of the conditions that determine the activation of the arching effect.

wall.

This arching effect is previously reported in the literature [49,50] and documented in Eurocode 6 [51]. To quantify the increase of frictional force resistance determined by the arching effect,  $F_{af}$ , a mechanical model already reported in the literature that includes both the Coulomb friction and arching effect contributions, is considered. The model is also used to analyse the contributions of these two mechanisms to the masonry pocket connections. In this model, the total frictional capacity consists of the cohesion and friction between timber and masonry and the additional out-of-plane strength (arching force). A number of parameters are required to compute the total capacity:

- the friction coefficient,
- the cohesion,
- the normal force acting on the topside and underside of the embedded part of the joist,
- the arching force due to the OOP displacement of the inner leaf, computed as described above.

The total shear strength of the connection is hence obtained as the sum of different contributions. The shear force capacity, which is the measured as the force at peak,  $F_{EP}$ , is divided by the upside and downside contact surface between the joist and the mortar, and is therefore obtained according to Coulomb's law:

$$\tau = \frac{F_{EP}}{2 \cdot t_w \cdot t_j} = c + \mu \cdot \sigma_N + \mu \cdot \sigma_A \quad (11)$$

where  $\tau$  is the shear strength,  $c$  is the cohesion,  $\mu$  is the friction coefficient,  $\sigma_N$  is the normal stress at the interface due to the initial pre-compression load, and  $\sigma_A$  is the additional normal stress at the interface caused by the arching effect. The cohesion is assumed to fully contribute to the reaction force until the achievement of the peak force, assuming an uncracked interface between joist and mortar. The normal stress due to the initial axial forces,  $\sigma_N$  is computed as the initial pre-compression load acting at the joist-wall connection,  $N_{if}$ , divided by the contact area. The normal stress due to arching,  $\sigma_A$ , is computed as the additional vertical force due to the arching action in the inner leaf,  $N_{af}$ , again divided by the contact area.

$$\sigma_N = \frac{N_{if}}{t_w \cdot t_j} \quad (12)$$

$$\sigma_A = \frac{N_{af}}{t_w \cdot t_j} \quad (13)$$

where  $t_w$  is the thickness of the inner leaf and  $t_j$  is the thickness of the joist. A method to estimate the values of the initial pre-compression

load,  $N_{if}$ , and of the additional vertical force,  $N_{af}$ , is described in the following subparagraphs.

(1) Initial pre-compression load ( $N_{if}$ )

The initial force acting on the contact areas between the joist and the masonry is determined as the sum of the weight of the masonry above the pocket, the overburden force at the top of the wall, and half of the vertical load applied to the joist, halfway between the pocket and the restrained end.

(2) Additional vertical force due to the arching effect ( $N_{af}$ )

An additional compressive stress due to arching may be created by the rotation of the wall blocks that form above the mid-height horizontal crack after rocking initiation in case of vertically restrained conditions. As these blocks rotate, the contact area between the joist and masonry reduces. In order to compute the arching force,  $N_{af}$ , the additional compressive stress,  $f_s$ , and the corresponding effective section depth,  $x$ , should be firstly calculated. The additional compressive stress at the contact area between the joist and the masonry due to the arching effect,  $f_s$ , is determined based on the study of Paulay and Priestley [32] by using Eq. (2) for a given OOP displacement of the inner leaf,  $u$ . The effective section depth,  $x$ , for the corresponding OOP displacement of the inner leaf can be computed as follows:

$$x = 3 \left( \frac{t_w}{2} - e - u \right) \quad (14)$$

where  $e$  is the eccentricity, and  $u$  is the OOP displacement of the inner leaf, in which used to calculate the additional compressive stress. The arching force on the joist is consequently computed assuming a triangular stress profile, as described in [32], as follows:

$$C = \frac{f_s \cdot x}{2} \quad (15)$$

$$N_{af} = C \cdot t_j \quad (16)$$

where  $C$  is the thrust force per unit width of the joist and  $t_j$  is the width of the joist. A schematic representation of arching effect is

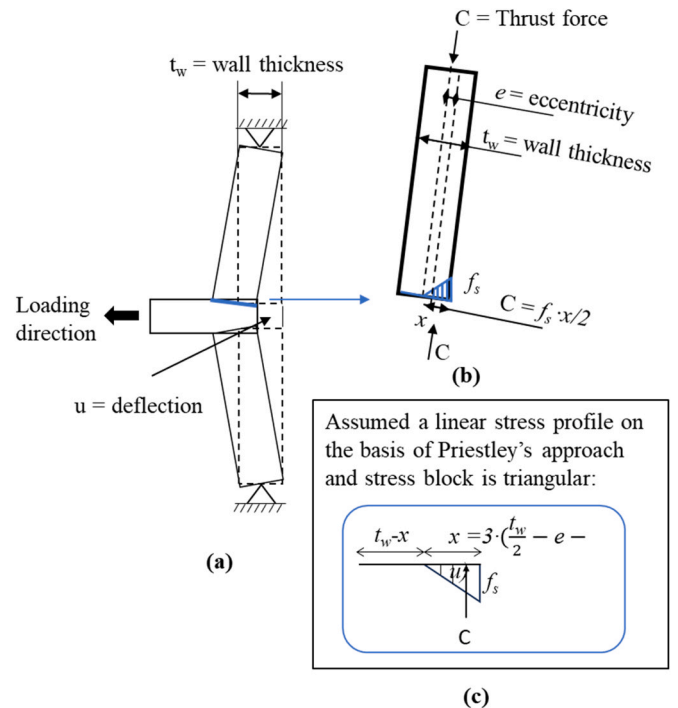


Fig. 11. Schematic view illustrating the arching effect: cavity wall with timber joist subjected to OOP displacement (a), idealized wall segment model based on Drysdale & Hamid [52](b) and equivalent stress block of masonry based on Eurocode 6 [51](c).

illustrated in Fig. 11.

It is important to note that the peak OOP deflection of the inner leaf is observed with increasing amplitude until failure of bond between joist and masonry, followed by its decrease and the simultaneous increase in joist sliding.

### 3.2. Wall rocking failure mode due to joist movement

When the joist is connected to the wall by additional connections, such as existing hook anchors, or via strengthening solutions, the connection between the structural components is more effective. The force capacity of the wall-joist connection increases largely and the structural system eventually fails due to OOP rocking of the wall. The model proposed by Tomassetti et al. [34] is used to predict the rocking capacity of the cavity wall system.

In order to analyse the behaviour of walls with different boundary conditions, the model proposed by Tomassetti et al. [34] takes into account both fixed-fixed and pinned-pinned configurations, defining the degree of moment restraint associated with the related top and bottom extremities,  $\alpha_t$  and  $\alpha_b$ , as shown in Fig. 12. In the experiments conducted by the authors [10], the boundary condition of the inner leaf is defined as pinned-pinned, while the outer leaf is considered as a cantilever wall. Regarding the inner leaf, the values of  $\alpha_t$  and  $\alpha_b$  are set equal to 0, indicating the development of the moment capacity with a fully developed crack in the middle of the wall. In this case, as seen in Fig. 12, the rocking behaviour develops around the crack (Point A\*), where  $\beta$  is equal to a value of 5.

The simplified envelope force-displacement curve introduced in Fig. 9 is therefore updated by adding the OOP rocking failure mode, as shown in Fig. 13. The vertical axis indicates the OOP force transferred by the timber joist to the wall, while the horizontal axis indicates the relative displacement between the joist and the wall. A bi-linear idealisation is used to define the rocking  $F-\Delta$  curve. Since the additional overburden due to the arching effect determined an increase of the frictional capacity, the failure of the system should be close to the OOP rocking capacity. It should be noted that, in reality, the size of actual walls is usually larger than those tested in this experimental campaign [10], and in this case more joists would be inserted in the wall. Since the size effect is not included in this study, the strength capacity may differ with the increasing of the wall size. Hence, the results of the rocking failure mode are constrained by the dimensions of the specimens used here.

The formulation, based on the rigid body theorem, can be used to

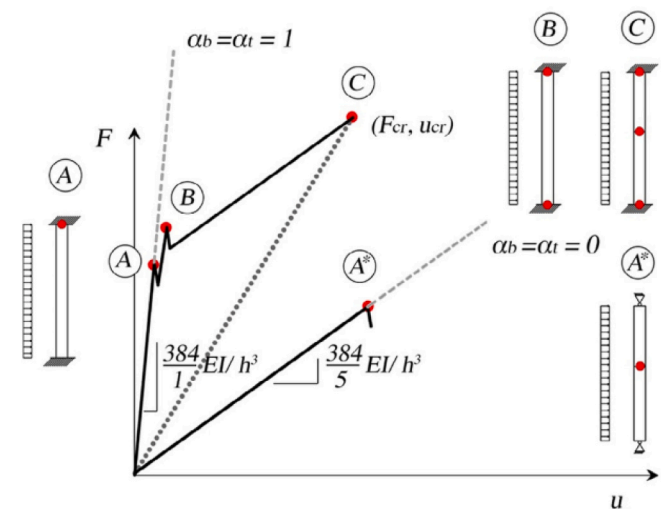


Fig. 12. Pre-cracking phase for one-way vertical spanning strip walls considering the two limit boundary condition situations which are fixed-fixed (A-B-C) and pinned-pinned (A\*) from Tomassetti et al. [34].

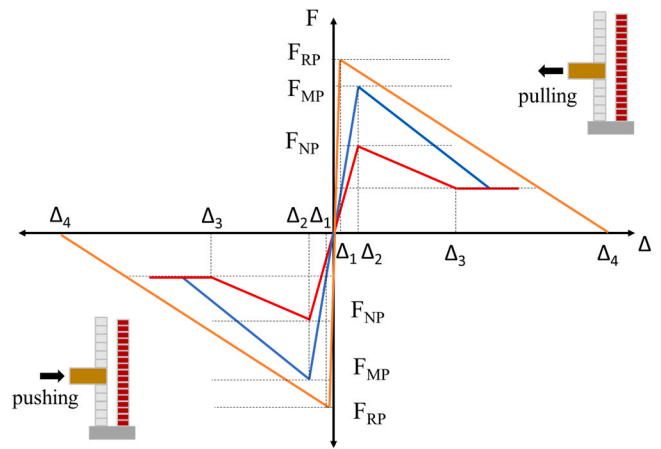


Fig. 13. Simplified envelope curve for both failure modes: the red line indicates the Coulomb friction law. The blue line is the proposed curve to predict the joist-sliding failure mode, including the Coulomb friction criterion and the arching effect. The orange line is the bilinear curve to predict the rocking capacity of the cavity wall system.

define an upper bound for the experimental results discussed in Arslan et al. [10] on the as-built and strengthened timber-joist cavity-wall specimens.

### 4. Comparison of predictions with the experimental tests

The force capacities predicted via the analytical models described in the previous sections are compared to the results of the experiments conducted by the authors and presented in [10]. Comparisons between the experimental and analytically determined values are presented in the following by clustering the results based on the failure mode. For example, the specimens with masonry pocket connection all exhibited joist-sliding failure mode, while those with hook anchor and the strengthened specimens all exhibited a rocking failure mode.

Friction between the joist and the masonry is an important parameter when calculating the joist force capacity. The masonry pocket connections are used for predicting the friction coefficient since the capacity of the connection was mainly governed by the friction. Hence, the friction coefficient is calculated as 0.6 and used for all other specimens as well, based on the last cycles of loading for both loading directions. This value is also in line with the experimental outcomes from testing campaign conducted on similar connections [45].

In order to define another important parameter of the analytical model, cohesion, it is necessary to determine the values of the total shear stress and the normal stresses due to the initial axial loading and arching. The total shear stress is computed based on the first part of Eq. (11), where the peak force,  $F_{EP}$ , is measured experimentally in either the pulling or pushing direction. The reason why the total shear stresses are separately computed for the pulling and pushing directions is due to the asymmetry in the test results. This asymmetry is attributed to the nonlinearity of the cavity wall system with the test setup, which caused additional vertical forces coming from the arching action of the inner leaf, hence different frictional resistance in pulling and pushing. The values of the normal stresses are computed via Eq. (12) and Eq. (13), respectively, where the additional vertical force due to the arching effect is derived via Eqs. (14)-(16). The values of cohesion are then computed via the second part of Eq. (11).

The values of cohesion computed for Specimen J1, J3 and J5 are equal to 0.10 MPa, 0.11 MPa and 0.08 MPa. A cohesion of 0.1 MPa can be determined not only directly based on the average behaviour reflected by Eq. (11) but also obtained as a reference value for the cohesion of masonry, as found in the literature [51,53-55]. Hence, to calibrate the mechanical model for the timber-masonry connections studied in the

considered campaign, a value of cohesion equal to 0.1 MPa is recommended. If a constant value of cohesion is then assumed, Eq. (11) can be used to predict the total resistance of the connection, while Eqs. (12)–(16) to identify the contribution of each resisting mechanism.

It is essential to define the out-of-plane displacement of the inner leaf in order to compute the additional vertical force due to the arching action in the inner leaf. Hence, the horizontal displacement of the middle height of the inner leaf of each specimen is determined, highlighting the initial rocking behaviour due to bonding and friction between the joist and masonry. It was obtained that the out-of-plane displacement at the middle of the inner leaf where the joist was inserted ranged from around 1 mm to 5 mm, in which the peak force was measured. The OOP rocking mechanism was activated not only due to the connectivity between timber and masonry and the two leaves but also due to the test setup, causing additional vertical forces due to the arching effect.

Regarding the rocking failure mode, the parameters of the bilinear curve derived according to the procedure illustrated in Section 3.2 are determined by means of Eqs. (5)–(7). Either the eccentricity of the top axial load equal to zero (RB Mechanism) or to half of the wall thickness (RB\* Mechanism) is considered.

The experimental outcomes are hereinafter compared to the predictions defined via the mechanical models corresponding to the appropriate failure mode. The properties derived from the tests used in the mechanical model are summarized in Table 1. The timber class of the timber joists was defined as C24 [44]. It is important to note that while wood is an orthotropic material, meaning its properties can vary between the three principal planes, in this case, it was assumed that the applied stress on the timber joist was exclusively in the direction parallel to the grain of the timber joist and did not exceed the elastic limit. Although not observed during the experiments [10], local failures may be observed at the end of the joist, which is also perpendicular to the grains, especially when the joist is forced to rotate. The effect of such local failures may be more detrimental in reality if the joist is in an imperfect condition, for example, affected by severe moisture or other sorts of decay.

For the interface failure, the predicted resistance is compared to the measured peak force obtained for Specimens J1, J3, and J5 in terms of the corresponding error, as shown in Table 2. An error of up to 6 % is obtained, which is within an acceptable margin considering the complexities and the geometric nonlinearities of the test setup. It is interesting to note that the frictional force due to arching varies largely for each considered test, depending on the OOP displacements of the wallet, and it can contribute up to more than 50 % of the total connection resistance (Specimen J3, pulling direction).

With the exception of specimens J1, J3, and J5 (whose performance is discussed above), the experimental force-displacement curves are compared to the bilinear curves predicted for an OOP rocking failure mechanism. The values of the parameters defining the bilinear curves for all the tests are reported in Table 3.

The bilinear curves of the specimens with a hook anchor are plotted versus the experimental curves, considering the OOP displacement at

the middle height of the inner and outer leaves, as displayed in Fig. 14a and b, respectively. Also, all the retrofitted specimens, labelled as TJ1-TJ6, experienced rocking failure mode (Fig. 14c and d). The final collapse of the retrofitted specimens occurs due to the instability of the outer leaf, which reaches large displacements, as seen in Fig. 14d.

It should be noted that the bilinear curves are defined only for the lowest value of pre-compression level, i.e. 0.1 MPa. In fact, although the model predicts that an increase in the pre-compression level leads to a significant increase in the total rigid force,  $F_{RP}$ , all the experimental curves remain below the selected analytical curve, showing small sensitivity of the system to the level of pre-compression applied at the beginning of the test.

As highlighted above, while masonry pocket connections lacking appropriate wall-to-floor connections exhibited frictional behaviour of the joist-wall interface, the resistance of all the other specimens is limited by the rocking of the wallets. This observation is confirmed not only by the experimental results but also by the results of the mechanical model prediction, which shows that the capacity predicted by the rocking behaviour of the wall,  $F_{RP}$ , is larger than that of a masonry pocket connection,  $F_{MP}$ , that exhibits joist-sliding failure mode, which leads to local failure. The computed peak force for the rocking mechanism represents, therefore, the upper limit to the resistance of the joist-wallet coupled system.

## 5. Conclusions

This paper aims to identify a mechanical model that is able to estimate the force capacity of timber-joist connections and identify the contribution of different resisting mechanisms. The adopted mechanical model examines two distinct failure modes: failure at the joist-to-wall interface, with joist-sliding and partial joist-to-wall interaction and the out-of-plane (OOP) rocking behaviour of the masonry walls.

The joist-to-wall interface failure, which involves joist-sliding and a partial joist-to-wall interaction mechanism, governs weak joist-masonry connections. Conversely, if the joist-masonry connection is strong, i.e. the connection is retrofitted or characterised by high strength, the failure mechanism shifts from the connection to the wall system, and the structural capacity is then reached due to the rocking behaviour of either one or both the leaves of the wallet.

This paper addresses two crucial factors: frictional behaviour and arching effect. These factors are present in real buildings and should be taken into account. Frictional behaviour pertains to the resistance between the timber joists and the masonry wall interface. In the latter case, even when the vertical displacement of walls is not restrained, the arching effect due to the out-of-plane behaviour of masonry walls, especially at lower levels, needs to be evaluated. This is due to the increased structural load, resulting in greater vertical pressure and possible arching effect.

An interesting finding is that, due to the OOP displacement of the masonry wall generated by the displacement imposed by the timber joist, an arching effect is activated, causing additional friction of the sliding joist. The total connection capacity at the interface between the joist and the wall should, therefore, include two frictional contributions: the initial friction force and the additional friction caused by the arching effect.

The considered model presented in this paper is capable of accurately predicting the peak capacity of the joist connection as obtained from the experimental campaign conducted by the authors. Specifically, the error between the analytical model and the experimental results for the specimens without hook anchors amounts to approximately 5 % in terms of peak forces in pulling and pushing if the values of friction coefficient and cohesion are assumed equal to 0.6 and 0.1 MPa, respectively. Additionally, it successfully defines the contribution of each mechanism in terms of the resistance at failure for the joist-to-wall interface failure. Remarkably, the frictional force due to arching can contribute up to more than 50 % of the total connection resistance and

**Table 1**  
Summary of joist-masonry connection properties.

Material Characteristic	Inner leaf	Outer leaf
Elastic modulus from Jafari[17] (MPa)	2749	5019
Friction coefficient between joist and masonry	0.6	-
Masonry weight above the joist (kN)	0.06	-
Overburden force above the joist (kN)	0.6	-
Height of wall (mm)	1030	950
Width of wall (mm)	930	930
Thickness of wall (mm)	100	100
Compressive strength of wall from Jafari[17] (MPa)	5.93	-
Flexural strength of wall (MPa)	0.1	0.28
Density of wall (kg/m <sup>3</sup> )	1683	1740

**Table 2**

Values for each contribution predicted by means of the proposed mechanical model along with the corresponding error. The different components contributing to the total force (cohesive force and friction force due to both the initial normal force and the arching effect) are identified.

Specimen	Cohesion (kN)		Initial frictional force (kN)		Frictional force due to arching (kN)		Predicted total force (kN)		Error	
	Pulling & pushing		Pulling & pushing		Pulling	Pushing	Pulling	Pushing	Pulling	Pushing
J1	1.20		1.09		0	0.78	2.29	3.07	0.1 %	-1.7 %
J3	1.20		1.09		1.66	3.05	3.95	5.34	-1.8 %	-4.4 %
J5	1.20		2.53		0.2	1.43	3.93	5.16	4.2 %	5.6 %

**Table 3**

Parameters used to define the bilinear curves for rocking failure of the tested specimens.

Specimen	$F_{cr}$ (kN)	$u_{cr}$ (mm)	$h_1/h$	$F_{RP}$ (kN)	$F_{RP}^*$ (kN)	$F_c$ (kN)	$u_{ins}$ (mm)	$u_{ins}^*$ (mm)
J1-J2 TJ1-TJ2	6.19	0.13	0.51	6.81	8.66	0.2	76.5	100
J3-J4 TJ3-TJ4	6.39	0.13	0.51	7.01	8.86	0.4	76.5	100
J5-J6 TJ5-TJ6	8.80	0.13	0.51	17.84	23.31	0.4	75.4	100

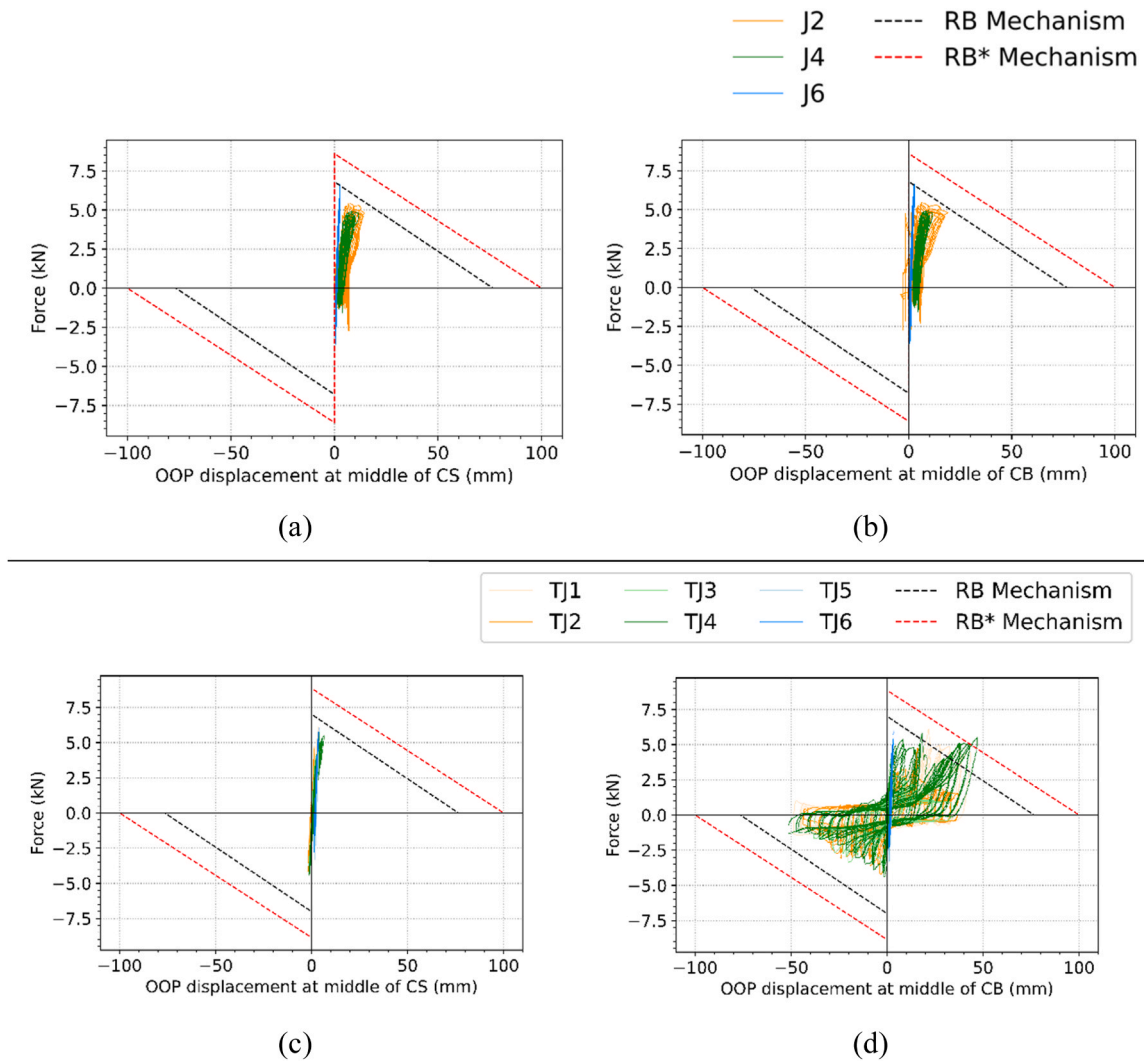


**Fig. 14.** Comparison between the test results of hook anchor specimens and the corresponding bilinear curves: force versus the OOP displacement at the middle height of the inner, CS, (a) and of the outer, CB, (b) leaves. Comparison between the test results of retested specimens and the corresponding bilinear curves: force versus the OOP displacement at the middle height of the CS (c) and of the CB (d) leaves.

should, therefore, not be neglected when vertical confinement of the connections is expected.

Regarding the rocking behaviour, the bilinear curve defined according to the method defined by Tomassetti et al. [34] effectively predicts the capacity of the structural system.

In closing, the mechanical models that were studied in this paper can be used as a basis not only to develop a general load-deformation hysteretic numerical model for timber-joint connections but also to be employed to simulate full-scale masonry cavity walls with timber diaphragms in which the connection details are explicitly taken into account.

### Declaration of Competing Interest

The authors declare that they have no known competing financial interests or personal relationships that could have appeared to influence the work reported in this paper.

### Appendix

List of symbols.

$F_{af}$  Frictional force caused by arching effect.

$F_{co}$  Cohesive force.

$F_{if}$  Frictional force caused by initial pre-compression.

$F_{ND}$  Initial total force due to initial pre-compression and cohesion.

$F_{MP}$  Total force determined by the mechanical model due to initial pre-compression, cohesion and arching effect.

$F_{RP}$  Total rigid body force due to rocking behaviour.

$F_{EP}$  Peak force measured experimentally.

$N_{af}$  Additional vertical force.

$N_{if}$  Initial pre-compression load.

$C$  Thrust force per unit width of joist.

$c$  Cohesion along the embedded part of joist in masonry wall.

$e$  Eccentricity.

$t_j$  Thickness of the joist.

$t_w$  Thickness of the inner leaf.

$\Delta$  Horizontal displacement of the inner leaf due to the joist.

$\sigma_N$  Normal stress on joist due to the initial axial forces.

$\sigma_A$  Normal stress on joist due to arching.

### References

- Lourenço PB, Mendes N, Ramos LF, Oliveira DV. Analysis of masonry structures without box behavior. *Int J Archit Herit* 2011;5:369–82. <https://doi.org/10.1080/15583058.2010.528824>.
- C. Blasi , A. Borri , S. Di Pasquale , P. Malesani , G. Nigro , A. Parducci , et al. , *Manuale per la riabilitazione e la ricostruzione sismica degli edifici — Regione dell'Umbria, DEI Tipografia del Genio Civile, Roma (in Italian), 1999.*
- D'Ayala DF, Paganoni S. Assessment and analysis of damage in L'Aquila historic city centre after 6th April 2009. *Bull Earthq Eng* 2011;9:81–104. <https://doi.org/10.1007/s10518-010-9224-4>.
- Moon L, Dizhur DY, Senaldi I, Derakhshan H, Griffith MC, Magenes G, et al. The demise of the URM building stock in Christchurch during the 2010–2011 Canterbury Earthquake Sequence. *Earthq Spectra* 2014;30:253–76. <https://doi.org/10.1193/022113EQS044M>.
- Dizhur DY, Dhakal RP, Bothara J, Ingham JM. Building typologies and failure modes observed in the 2015 Gorkha (Nepal) earthquake. *Bull N Zeal Soc Earthq Eng* 2016;49:211–32. <https://doi.org/10.5459/bnzsee.49.2.211-232>.
- van Eck T, Goutbeek F, Haak H, Dost B. Seismic hazard due to small-magnitude, shallow-source, induced earthquakes in The Netherlands. *Eng Geol* 2006;87:105–21. <https://doi.org/10.1016/j.enggeo.2006.06.005>.
- Kallioras S, Guerrini G, Tomassetti U, Marchesi B, Penna A, Graziotti F, et al. Experimental seismic performance of a full-scale unreinforced clay-masonry building with flexible timber diaphragms. *Eng Struct* 2018;161:231–49. <https://doi.org/10.1016/j.engstruct.2018.02.016>.
- Kallioras S, Correia AA, Graziotti F, Penna A, Magenes G. Collapse shake-table testing of a clay-URM building with chimneys. *Bull Earthq Eng* 2020;18:1009–48. <https://doi.org/10.1007/s10518-019-00730-0>.
- Moshfeghi A, Smyrou E, Arslan O, Bal IE. Out-of-plane shake table tests on solid masonry walls with timber floors. *Structures* 2024.
- O. Arslan, F. Messali, E. Smyrou, I.E. Bal, J.G. Rots, Cyclic load response of timber joists in double-leaf masonry cavity walls – Part 1: Experimental results (2024).
- Suh NP, Turner PL. *Elements of the Mechanical Behaviour of Solids*. Scripta Book Co; 1975.
- K. Doherty, An investigation of the weak links in the seismic load path of unreinforced masonry buildings, (2000) 354.
- Griffith M, Page A. On the seismic capacity of typical DPC and slip joints in unreinforced masonry buildings. *Aust J Struct Eng* 1998;1:133–40.
- Casapulla C, Argiento L, da Porto F, Bonaldo D. The relevance of frictional resistances in out-of-plane mechanisms of block masonry structures. in: *Proc. 16th Int. Brick Block Mason. Conf. Padova, Italy: CRC Press; 2016. p. 145–54.* (<https://www.taylorfrancis.com/books/9781498795920/chapters/10.1201/b21889-16>).
- Almeida JP, Beyer K, Brunner R, Wenk T. Characterization of mortar–timber and timber–timber cyclic friction in timber floor connections of masonry buildings. *Mater Struct* 2020;53:51. <https://doi.org/10.1617/s11527-020-01483-y>.
- Morandi P. Second order effects in out-of-plane strength of URM walls subjected to bending and compression. *ROSE Sch* 2006. <https://doi.org/10.13140/RG.2.2.19870.64326>.
- S. Jafari, Material characterisation of existing masonry: A strategy to determine strength, stiffness and toughness properties for structural analysis, 2021. <https://doi.org/10.4233/uuid:3bcbbc72-0212-44e9-ac86-2fdc54ec5987>.
- Rahman A, Ueda T. Experimental investigation and numerical modeling of peak shear stress of brick masonry mortar joint under compression. *J Mater Civ Eng* 2014;26. [https://doi.org/10.1061/\(ASCE\)MT.1943-5533.0000958](https://doi.org/10.1061/(ASCE)MT.1943-5533.0000958).
- Pelà L, Kasioumi K, Roca P. Experimental evaluation of the shear strength of aerial lime mortar brickwork by standard tests on triplets and non-standard tests on core samples. *Eng Struct* 2017;136:441–53. <https://doi.org/10.1016/j.engstruct.2017.01.028>.
- Kallioras S. Numerical simulation of shaking table tests on a URM cavity-wall building. *Mason Int* 2017;30(2).
- Y. Endo, Y. Kondo, G. Iwanami, Adaptive Pushover Analyses of a Heritage Structure: Application to a Multi-Tiered Pagoda Temple, (2021). <https://doi.org/10.23967/sahc.2021.020>.
- Coulomb C. Sur une application des règles maximis et minimis a quelques problèmes de statique, relatives a l'architecture. *Acad Sci Paris Mem Math Phys* 1776; 7343–382.
- Priestley MJN. Seismic behaviour of unreinforced masonry walls. *Bull N Zeal Soc Earthq Eng* 1985;18:191–205. <https://doi.org/10.5459/bnzsee.18.2.191-205>.
- Flanagan RD, Bennett RM. Arching of masonry infilled frames: comparison of analytical methods. *Pract Period Struct Des Constr* 1999;4:105–10. [https://doi.org/10.1061/\(ASCE\)1084-0680\(1999\)4:3\(105\)](https://doi.org/10.1061/(ASCE)1084-0680(1999)4:3(105)).
- Walsh K, Dizhur DY, Giongo I, Derakhshan H, Ingham JM. Predicted versus experimental out-of-plane force-displacement behaviour of unreinforced masonry walls. *Structures* 2018;15:292–306. <https://doi.org/10.1016/j.istruc.2018.07.012>.
- Derakhshan H, Dizhur DY, Griffith MC, Ingham JM. In situ out-of-plane testing of as-built and retrofitted unreinforced masonry walls. *J Struct Eng* 2014;140:04014022. [https://doi.org/10.1061/\(asce\)st.1943-541x.0000960](https://doi.org/10.1061/(asce)st.1943-541x.0000960).
- G. Magenes, Lecture on masonry structures (14.01.2020), Lecture, (2020).
- K. Angervo, Über die Knickung und Tragfähigkeit eines exzentrisch gedrückten Pfeilers ohne Zugfestigkeit unter- und oberhalb der Proportionalitätsgrenze mit besonderer Berücksichtigung des rechteckigen Quer- schnitts, (1954).
- K. Angervo, A.I. Putkonen, U. Attila, Erweiterung der Theorie der Biegung eines Pfeilers ohne Zugfestigkeit und ihre Anwendung zur Berechnung von Rahmentragwerken mit unbewehrten Stielen, (1957).
- Sahlin S. *Structural Masonry*. Prentice-Hall; 1971.
- CHAPMAN JC, SLATFORD J. The elastic buckling of brittle columns. (Includes Appendices). *Proc Inst Civ Eng* 1957;6:107–25. <https://doi.org/10.1680/iicep.1957.12395>.
- Paulay T, Priestley MJN. *Seismic Design of Reinforced Concrete and Masonry Buildings*. Hoboken, NJ, USA: John Wiley & Sons, Inc.; 1992. <https://doi.org/10.1002/9780470172841>.
- Griffith MC, Magenes G, MELIS G, PICCHI L. Evaluation of out-of-plane stability of unreinforced masonry walls subjected to seismic excitation. *J Earthq Eng* 2003;7:141–69. <https://doi.org/10.1080/13632460309350476>.
- Tomassetti U, Graziotti F, Penna A, Magenes G. Modelling one-way out-of-plane response of single-leaf and cavity walls. *Eng Struct* 2018;167:241–55. <https://doi.org/10.1016/j.engstruct.2018.04.007>.
- Derakhshan H, Griffith MC, Ingham JM. Airbag testing of multi-leaf unreinforced masonry walls subjected to one-way bending. *Eng Struct* 2013;57:512–22. <https://doi.org/10.1016/j.engstruct.2013.10.006>.
- Godio M, Beyer K. Analytical model for the out-of-plane response of vertically spanning unreinforced masonry walls. *Earthq Eng Struct Dyn* 2017;46:2757–76. <https://doi.org/10.1002/eqe.2929>.
- Tomažević M. Some considerations on testing and experimental simulation of seismic behaviour of masonry walls and buildings. in: *Proc. 16th Int. Brick Block Mason. Conf. Padova, Italy: CRC Press; 2016. p. 65–70.* (<https://www.taylorfrancis.com/books/9781498795920/chapters/10.1201/b21889-6>).
- Standards Australia, *Masonry Structures - AS3700-2001*, 2018.
- Doherty K, Griffith MC, Lam NTK, Wilson J. Displacement-based seismic analysis for out-of-plane bending of unreinforced masonry walls. *Earthq Eng Struct Dyn* 2002;31:833–50. <https://doi.org/10.1002/eqe.126>.
- Simsir CC, Aschheim MA, Abrams DP. Out-of-plane dynamic response of unreinforced bearing walls attached to flexible diaphragms. *Proc 13th World Conf Earthq Eng* 2004:15.
- Griffith MC, Lam NTK, Wilson JL, Doherty K. Experimental investigation of unreinforced brick masonry walls in flexure. *J Struct Eng* 2004;130:423–32. [https://doi.org/10.1061/\(asce\)0733-9445\(2004\)130:3\(423\)](https://doi.org/10.1061/(asce)0733-9445(2004)130:3(423)).

- [42] Vaculik J, Lumantarna E, Griffith MC, Lam NTK, Wilson J. Dynamic response behaviour of unreinforced masonry walls subject to out of plane loading. *Aust Earthq Eng Soc Conf* 2007.
- [43] Graziotti F, Tomassetti U, Penna A, Magenes G. Out-of-plane shaking table tests on URM single leaf and cavity walls. *Eng Struct* 2016;125:455–70. <https://doi.org/10.1016/j.engstruct.2016.07.011>.
- [44] Nederlands Normalisatie-instituut (NEN), NEN-EN 338:2013 - Structural timber - Strength classes, 2016.
- [45] Mirra M, Ravenshorst G, de Vries P, Messali F. Experimental characterisation of as-built and retrofitted timber-masonry connections under monotonic, cyclic and dynamic loading. *Constr Build Mater* 2022;358:129446. <https://doi.org/10.1016/j.conbuildmat.2022.129446>.
- [46] Magenes G. Masonry building design in seismic areas: recent experiences and prospects from a European standpoint, 1st. *Eur Conf Earthq Eng Seismol* 2006. Keynote 9.
- [47] Sorrentino L, Masiani R, Griffith MC. The vertical spanning strip wall as a coupled rocking rigid body assembly. *Struct Eng Mech* 2008;29:433–53. <https://doi.org/10.12989/sem.2008.29.4.433>.
- [48] ASCE/Sei 41-13. Seismic Evaluation and Retrofit of Existing Buildings. Reston, VA: American Society of Civil Engineers; 2014. <https://doi.org/10.1061/9780784412855>.
- [49] Morandi P, Magenes G, Griffith MC. Second order effects in out-of-plane strength of unreinforced masonry walls subjected to bending and compression. *Aust J Struct Eng* 2008;8:133–44. <https://doi.org/10.1080/13287982.2008.11464993>.
- [50] McDowell EL, McKee KE, Sevin E. Arching action theory of masonry walls. *J Struct Div* 1956;82. <https://doi.org/10.1061/JSDEAG.0000019>.
- [51] EN 1996-1-1–2005, Eurocode 6 – Design of masonry structures – Part 1–1: General rules for reinforced and unreinforced masonry structures, (2005).
- [52] Drysdale RG, Hamid AA, Baker LR. *Masonry Structures: Behavior and Design*. Englewood Cliffs, N.J: Prentice Hall; 1994.
- [53] Pereira JM, Correia AA, Lourenço PB. In-plane behaviour of rubble stone masonry walls: experimental, numerical and analytical approach. *Constr Build Mater* 2021; 271. <https://doi.org/10.1016/j.conbuildmat.2020.121548>.
- [54] Ghiassi B, Vermelfoort AT, Lourenço PB. Masonry mechanical properties. in: *Numer. Model. Mason. Hist. Struct.* Elsevier; 2019. p. 239–61. <https://doi.org/10.1016/B978-0-08-102439-3.00007-5>.
- [55] Rahgozar A, Hosseini A. Experimental and numerical assessment of in-plane monotonic response of ancient mortar brick masonry. *Constr Build Mater* 2017; 155:892–909. <https://doi.org/10.1016/j.conbuildmat.2017.08.079>.